RSC Advances

PAPER

View Article Online
View Journal | View Issue

Cite this: *RSC Adv.*, 2019, **9**, 3030

Comparison of transition metal (Fe, Co, Ni, Cu, and Zn) containing tri-metal layered double hydroxides (LDHs) prepared by urea hydrolysis†

Sajid Naseem, *[a] Bianca Gevers, [b] Regine Boldt, [a] Frederick J. W. J. Labuschagné [b] and Andreas Leuteritz[a]

Received 11th December 2018
Accepted 16th January 2019

DOI: 10.1039/c8ra10165e

rsc.li/rsc-advances

This paper details a successful synthesis and comparison of a range of tri-metal hydrotalcite-like layered double hydroxides (LDHs) using urea hydrolysis. Transition-metal-substituted MgMAl-LDHs were synthesized with M = Fe, Co, Ni, Cu or Zn. 5 mol% and 10 mol% substitutions were performed, where Mg was substituted with Co, Ni, Cu and Zn, and Al with Fe. The successful synthesis of crystalline MgMAl-LDHs was confirmed using X-ray powder diffraction (XRD) analysis. Energy-dispersive X-ray (EDX) spectroscopy was used to identify substituted metals and determine changes in composition. Changes in morphology were studied using scanning electron microscopy (SEM). Thermogravimetric analysis was used to determine the effect of Fe-, Co-, Ni-, Cu- or Zn-substitution on the thermal degradation of the MgMAl-LDH phase. The structure, morphology and thermal behavior of the LDHs were shown to be influenced by the substituted transition metals. The observed thermal stability took the order MgNiAl- > MgFeAl- = MgAl- ≥ MgCoAl- > MgCuAl- > MgZnAl-LDH. The urea hydrolysis method was shown to be a simple preparation method for well-defined crystallite structures with large hexagonal platelets and good distribution of transition metal atoms in the substituted LDHs.

Introduction

LDHs – known as hydrotalcite-like materials – are anionic clays with the formula

$$[M_{1-x}^{2+}M_x^{3+}(OH)_2]^{x+}\cdot[(A^{n-})_{x/n}\cdot yH_2O]^{x-} \quad (1)$$

where M^{2+}, M^{3+} and A^{n-} are divalent metal cations, trivalent metal cations and interlayer anions respectively.[1,2] The study of these materials has increased due to their wide range of applications and tunable properties.[3] The most studied applications of LDHs include their use as antioxidants,[4] stabilizers[5,6] and flame retardants for polymers,[7] photocatalytic materials,[8] and as UV-Vis absorption materials.[9] The possibility to intercalate organic compounds into the layers of the LDHs also make them useful for multifunctional applications, such as usage in dye sensitized solar cells, enhancement of flame retardant properties, and resistance to thermal degradation.[10–16] Most recently, the development of novel layered materials attracts great interest in various fields.[17–21]

There exist many techniques to prepare LDHs, the most common being co-precipitation, urea hydrolysis, ion exchange and hydrothermal synthesis.[2,22–24] LDHs can be prepared with a variety of metal combinations that can be tailored to the desired applications and can have different structural, chemical and photoelectric properties dependent on the incorporated metals and preparation methods.[25–30] It has been found that the inclusion of a third metal into the layer structure can modify the LDHs optical properties, UV-Vis light absorption range and catalytic properties.[31,33]

Kang *et al.* investigated how the catalytic oxidation of SO_2 to SO_3 can be improved through substitution of Fe and Mn in co-precipitated MgAl-LDHs.[32] Jabłońska *et al.* prepared MgCuFe-LDHs using co-precipitation and characterized the materials for use as catalysts for the selective catalytic oxidation of ammonia to nitrogen and water vapor.[34] Basąg *et al.* synthesized CuMgAl mixed metal oxides derived from LDHs through co-precipitation and studied these as catalysts for the selective oxidation of ammonia to dinitrogen. They concluded that the different molar ratios and calcination temperatures had an effect on the catalytic activity of the LDHs.[35] Wang *et al.* synthesized Zn-doped MgAl-LDHs through modified homogeneous co-precipitation and studied the effect of thermal ageing on PVC. It was found that Zn-based MgAl-LDHs enhance the thermal stability of PVC.[36] Chmielarz *et al.* synthesized MgAl, CuMgAl and FeMgAl mixed metal oxides derived from co-precipitated LDHs and

[a]*Leibniz-Institut für Polymerforschung Dresden e. V, Hohe Straße 6, Dresden, 01069, Germany. E-mail: naseem@ipfdd.de*

[b]*Department of Chemical Engineering, University of Pretoria, Lynwood Road, Pretoria, 0002, South Africa*

† Electronic supplementary information (ESI) available. See DOI: 10.1039/c8ra10165e

doped the catalysts with noble metals. The catalytic oxidation of ammonia to nitrogen was studied.[37] Parida *et al.* synthesized a ternary series of (Mg/Al + Fe)–CO_3 LDHs by co-precipitation and tested them in the photocatalytic hydrogen generation from water.[31] Kovanda *et al.* prepared CuMgAl-LDHs with different molar ratios *via* co-precipitation and studied their catalytic activity in toluene combustion.[38] Chmielarz *et al.* studied the influence of Cu, Co and Ni cations incorporated into hydrotalcite on the thermal decomposition of the material. The LDHs were synthesized using co-precipitation and the thermal behavior was shown to be influenced by the amount of Cu, Co and Ni substituted.[39] Kim *et al.* prepared ternary ZnAl-LDHs substituted with Co and Cu through co-precipitation and studied their photocatalytic effects in dye degradation.[40] Liu *et al.* studied FeCoAl- and ZnCoAl-LDHs with different metal ratios. Well defined crystals were formed.[41] Zheng *et al.* synthesized ZnMgAl-LDHs using a modified urea hydrolysis method and studied how the concentration of Zn affects the adsorption of methyl orange onto ZnMgAl-LDHs.[42] Chagas *et al.* synthesized MgCoAl- and NiCoAl-LDHs and characterized them using a variety of techniques.[43] Sakr *et al.* synthesized MgZnAl-LDHs using a modified urea hydrolysis method and discussed how different Zn concentrations can affect the capturing of carbon dioxide from methane streams.[44] Labuschagné *et al.* investigated the heat stabilization of flexible PVC with 25 mol% transition metal substituted MgFeAl-, MgCuAl-, and MgZnAl-LDH, synthesized using a hydrothermal method. They found that the inclusion of Zn in the MgAl-LDH improved the color retention and that MgCuAl-LDH acted as an HCl scavenger.[45]

These investigations are illustrative of the synthesis routes applied to tri-metal LDHs and the applications for which they have been investigated. However, as evident from the overview, and illustrated in Table 1, the synthesis of these materials has been dominated by co-precipitation. In addition to this, the influence of transition metal content on the morphology and thermal degradation of LDHs has not yet been thoroughly investigated – importantly, a comparison between the different transition-metal-substituted MgAl-LDH synthesized at the same conditions is lacking.

Although infrequently used for tri-metal LDH synthesis (as shown in Table 1) urea hydrolysis can provide LDHs with large, thin platelets and narrow particle size distributions. This stands in contrast to the LDHs synthesized by co-precipitation, which typically require extensive ageing to have similar characteristics. LDHs containing the transition metals Fe, Co, Ni, Cu and Zn as substituted metals in MgAl-LDH, have – to our knowledge – not been investigated comprehensively. It is, therefore, the aim of this paper, to provide the reader with a method to synthesize MgMAl-LDHs and compared the properties with M = (Fe, Co, Ni, Cu, Zn) using urea hydrolysis. Furthermore, this paper serves to illustrate the changes in crystallinity and morphological- and thermal properties between the different transition-metal-substituted LDHs as well as with an increase in the transition metal content.

Experimental techniques and characterization

Materials

Chemically pure (CP) or analytical grade (AR) reactants were used for all experiments without further treatment. $Mg(NO_3)_2 \cdot 6H_2O$, $Al(NO_3)_3 \cdot 9H_2O$, $Fe(NO_3)_3 \cdot 9H_2O$, $Co(NO_3)_2 \cdot 6H_2O$, $Ni(NO_3)_2 \cdot 6H_2O$, $Cu(NO_3)_2 \cdot 3H_2O$, $Zn(NO_3)_2 \cdot 6H_2O$ were purchased from ABCR. Urea was purchased from Sigma Aldrich. Distilled water was used for all experiments.

Synthesis of LDHs

MgMAl-LDHs were synthesized using urea hydrolysis as explained in literature.[22] A $M^{II+} : M^{III+}$ molar ratio of 2 : 1 was used for all LDHs. The transition metals were substituted as follows: M/(Mg + M) = 0.05, 0.1 for Co, Ni, Cu and Zn and M/(Al + M) = 0.05, 0.1 for Fe (all on a molar basis). Salt solutions of $Mg(NO_3)_2 \cdot 6H_2O$ and $Al(NO_3)_3 \cdot 9H_2O$ with the required amounts of Fe, Co, Ni, Cu and Zn salts were prepared in distilled water, mixed in a round bottom flask, and heated to 100 °C, at which temperature they were kept for 48 h. After the reaction mixture was cooled down to room temperature, the slurry was filtered and washed with distilled water. The filter cake was dried in an oven at 70 °C for 24 h. The synthesized LDHs will be designated the following naming convention: MgMAl-x with M = Fe, Co, Ni, Cu, Zn and x = 5 (5% molar substitution) and 10 (10% molar substitution) of Mg or Al.

Characterization methods

X-ray diffraction measurements were performed on a Panalytical X'Pert PRO X-ray diffractometer in θ–θ configuration, equipped with a Fe filtered Co-Kα radiation (1.789 Å) and with an X'Celerator detector and variable divergence- and fixed receiving slits. Samples were prepared according to the standardized Panalytical backloading system, which provides nearly random distribution of the particles. The data was collected in the angular range $5° \leq 2\theta \leq 80°$ with a step size 0.008° 2θ and a 13 s scan step time. The phases were identified using X'Pert Highscore plus software. Scanning electron microscopy (SEM) images were taken with a Zeiss Ultra Plus. Energy dispersive X-ray Spectroscopy (EDX) was done with a QUANTAX FlatQUAD from Bruker Nano GmbH. SEM samples were prepared by distributing the LDHs on a stub and sputter coating them with 3 nm of platinum. SEM micrographs were taken at 4.00 kV. For SEM-EDX analysis the samples were deposited on an Au-TEM-Grid with a 2 nm Au-holey-film. The samples were coated with carbon before measurement. EDX studies were performed with an accelerating voltage of 12 keV. Thermogravimetric analysis (TGA) was performed with a heating rate of 10 °C min^{-1} using a TGA Q5000 from TA instruments in an inert nitrogen atmosphere in the temperature range of 25–1000 °C. TGA measurements were performed three times and the mean value with the corresponding standard deviation is shown in the results.

Table 1 Previously reported tri-metal LDHs using urea hydrolysis and co-precipitation where a range of metal ratios was investigated (subs. M, M = substituted metal)

LDH	Subs. M	Variations	Method	Characterization methods	Ref.
(Mg/Al + Fe)–CO_3	Fe	Mg : (Al + Fe) = 2 : 1	Co-precipitation	PXRD, FTIR, TGA, DTA, UV-Vis, BET, TEM, XPS	31
MgAlFe, MnMgAlFe	Fe, Mn	0% wt, 1% wt, 5% wt and 10% wt	Co-precipitation	XRD, FTIR, TGA, DSC, catalytic test	32
MgCuFe	Cu	2 : 1 : 1, 2 : 0.5 : 1 and 2 : 0 : 1	Co-precipitation	XRD, catalytic tests	34
CuMgAl	Cu	5 mol% Cu, temperature variations (600 °C, 700 °C and 800 °C)	Co-precipitation	XRD, FTIR, EPMA, TGA-DTG-QMS, BET, catalytic tests, DRUV-Vis	35
MgZnAl	Zn	2 : 0 : 1, 1.7 : 0.3 : 1.0, 1.5 : 0.5 : 1.0, 1.3 : 0.7 : 1.0, 1.0 : 1.0 : 1.0	Homogeneous Co-precipitation	XRD, FTIR, TEM, SEM, TG-DTA	36
MgAl, CuMgAl, FeMgAl	Cu, Fe	71 : 29, 5 : 66 : 29, 5 : 66 : 29 (atomic ratios)	Co-precipitation	XRD, UV-vis-DRS, TG-DTA-QMS, STEM, BET, redox properties	37
CuMgAl	Cu	0 : 4 : 2, 1 : 3 : 2, 2 : 2 : 2, 3 : 1 : 2, and 4 : 0 : 2	Co-precipitation	XRD, TG, DTA, BET, TPD, catalytic activity	38
MMgAl–CO_3–NO_3	Cu, Co, Ni	M : Mg (0.10 : 0.61) and M : Al (0.10 : 0.29)	Co-precipitation	High temperature XRD, TGA-DTA-MS, TPR	42
ZnAl, ZnCuAl, ZnCoAl	Cu, Co	2 : 1, 1.9 : 0.1 : 1, 1.75 : 0.25 : 1, 1.5 : 0.5 : 1, 1 : 1 : 1	Co-precipitation	XRD, FTIR, Raman spectroscopy, UV-Vis, TEM, photocatalytic activity	40
MgCoAl, MgNiAl, MgCuAl	Co, Cu, Ni	M(II) : Mg(II) : Al(III) 1 : 6 : 2	Co-precipitation	XRD, XRF, TG MSD, FTIR and Raman spectroscopy	46
MgAl, MgCoAl, MgNiAl, MgFeAl	Fe, co, Ni	$MgCl_2 \cdot 6H_2O = 0.29AlCl_3 \cdot 6H_2O = 0.1$, $CoCl_2 = 0.01$, $FeCl_2 \cdot 4H_2O = 0.01$, $NiCl_2 \cdot 6H_2O = 0.01$	Co-precipitation	PXRD, EXAFS, XANES, FTIR, SEM-EDX, TGA	47
MgCoAl, NiCoAl	Mg, Ni	Molar ratios $M^{2+} : M^{3+}$ of 2 ($x = 1 : 3$)	Urea hydrolysis	XRD, NMR, TGA-DTA, FTIR, SEM and N_2 adsorption–desorption	43
ZnMgAl	Zn	(Zn + Mg) : Al = 2 : 1, Zn/Mg = 0, 0.125, 0.5 and 0.8	Modified urea hydrolysis with co-precipitation	XRD, SEM, FTIR, UV-Vis, AAS	42
MgZnAl	Mg, Zn	((Mg + Zn)/Al molar ratio = 5.67), MgZn (25 : 75) Al, MgZn (50 : 50) Al, MgZn (75 : 25) Al	Modified urea hydrolysis with co-precipitation	XRD, FTIR, TGA, DTA, elemental analysis, SEM and TEM	44
FeCoAl, ZnCoAl	Fe, Zn	M/(M + Co) = 0.8, 0.5, 0.2	Urea hydrolysis	XRD, SEM and UV-Vis	41
MgFeAl, MgCuAl, MgZnAl	Fe, Cu, Zn	25 mol%	Hydrothermal	XRD, SEM, BET, particle size, ICP-OES, FTIR, TGA, dynamic heat stability, thermal stability	45

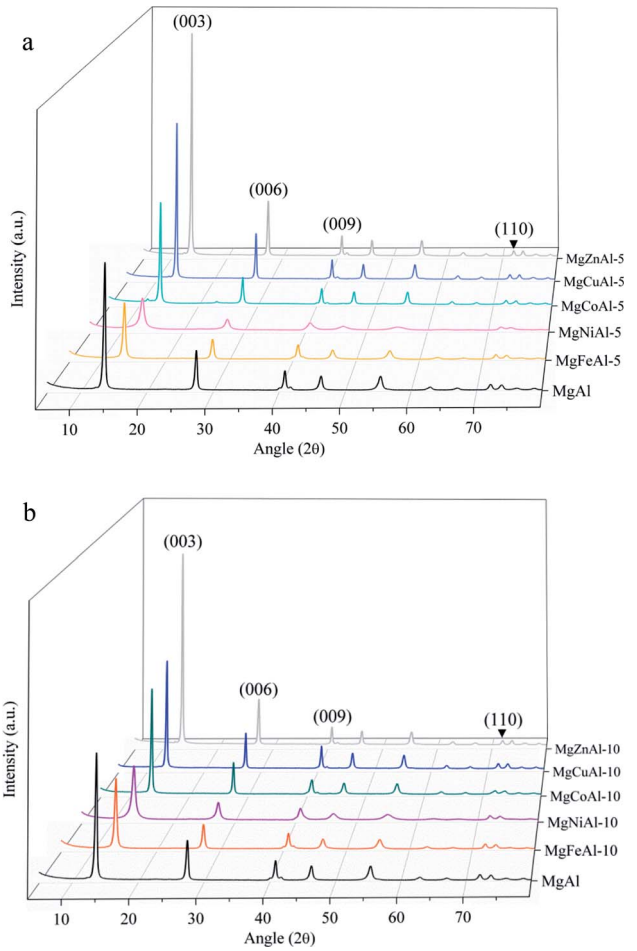

Fig. 1 (a) XRD patterns obtained for the series of M = (Fe, Co, Ni, Cu, Zn) (5 mol%) substituted tri-metal MgMAl-LDHs and MgAl-LDH synthesized using urea hydrolysis. (b) XRD patterns obtained for the series of M = (Fe, Co, Ni, Cu, Zn) (10 mol%) substituted tri-metal MgMAl-LDHs and MgAl-LDH synthesized using urea hydrolysis.

Results and discussion

X-ray diffraction (XRD)

The XRD patterns of the synthesized LDHs are shown in Fig. 1(a and b). The reflections are narrow and very few to no contaminants or side products could be observed, indicating almost complete substitution of Fe, Co, Ni, Cu, and Zn into the crystalline MgAl-LDH structure.[42,43] A high intensity for the reflections corresponding to the (003), (006), (009) and (110) planes of a rhombohedral crystal lattice could be observed (as expected for materials based on a brucite structure), indicating a high orderliness and crystallinity of the samples.[5,48] High platelet crystallinity and orderliness is characteristic to the urea hydrolysis method used for synthesis.[22]

Clear changes in reflection intensity can be seen in Fig. 1(a and b). Apart from the Ni-substituted LDHs, the reflection intensity of the samples increased moving right on the periodic table. Because of phenomenon's such as constructive interference and preferred crystallite orientation observable in clays which can alter the sample reflection intensities,[49] an increase in reflection intensity cannot directly be related to an increase in sample crystallinity. An example of this would be a comparison of intensities between 5%- and 10% substituted LDHs as produced in this study. It is, however, expected that significantly increased reflection intensities as seen upon moving right on the periodic table upon 5 mol% and 10 mol% transition metal substitution in the LDHs (apart from Ni) can be correlated to increases in the sample crystallinity.

As the substitution increases, an amorphous phase can form, which, dependent on the amount of amorphous material present, can hinder further growth of crystals and in turn reduce the crystallinity of the LDHs.[31,39] SEM micrographs showed small amounts of unidentified material on the LDH platelets which we believe to be amorphous material and which will be designated as residue from hereon. The residue material is believed to consist of oxides of the metals used for synthesis. These phases would, due to the low intensity and broadened nature of their diffraction patterns, remain undetected (if their quantities are small enough)[31] or be detectable as amorphous halo's on the XRD graphs (if present in large amounts). It was, therefore, reasoned, that these phases existed in very small amounts that did not influence the XRD patterns substantially, and that the samples produced consisted mainly of the desired LDH phase. A schematic representation of the substitution of the transition metals into the LDH structure is shown in Fig. 2.

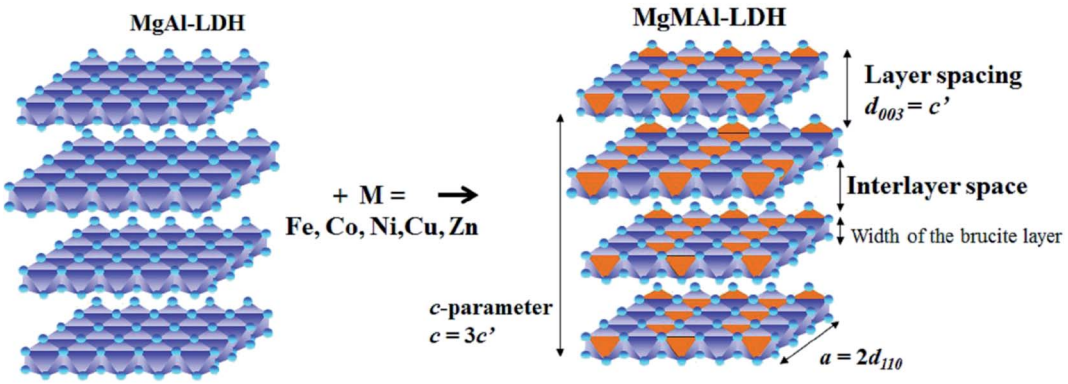

Fig. 2 Schematic representation of di-metal (MgAl) and tri-metal layered double hydroxides (LDHs)(MgMAl) where M = Fe, Co, Ni, Cu, Zn adapted from (ref. 17).

Table 2 Peak positions for the (003), (006) and (009) planes, interlayer distance (d_{003}), crystal lattice parameters (c and a) and Crystallite sizes of the MgMAl-LDHs with M = (Fe, Co, Ni, Cu, Zn) for 5% molar substitutions synthesized using urea hydrolysis

Sample ID	2θ (003) (°)	2θ (006) (°)	2θ (009) (°)	2θ (110) (°)	$d_{(003)}$ (Å)	c (Å)	a (Å)	D (nm)
MgAl	13.613	27.451	40.893	72.242	7.547	22.769	3.035	28.2
MgFeAl-5	13.569	27.385	40.870	72.155	7.572	22.815	3.038	20.8
MgCoAl-5	13.635	27.517	40.848	72.111	7.535	22.747	3.040	33.7
MgNiAl-5	13.503	27.319	40.826	72.132	7.609	22.878	3.039	11.4
MgCuAl-5	13.635	27.495	40.827	72.088	7.535	22.757	3.040	39.7
MgZnAl-5	13.635	27.473	40.783	72.067	7.535	22.771	3.041	39.5

The layer spacing (d-spacing) can be modified by changes in the anion or water content in the interlayer or changes in the LDH layer composition. The isomorphic replacement of Mg^{2+} with M = (Co, Ni, Cu, Zn) and Al^{3+} with M = (Fe) leads to a change in layer spacing if the ionic radius of the substituted metal is different to that of Mg or Al. This is observed by a shift in reflections on the XRD pattern against those obtained for plain MgAl-LDH and is regarded as an indication of the successful substitution of the transition metals.[31,32,50] Dependent on the radius of the substituted ion, the reflections shift to the left when a larger cation is substituted and to the right when a smaller cation is substituted.

The ionic radii used in the following discussion were based on a rhombohedral crystal lattice structure with VI coordination. Changes in layer distance were observed for Fe- and Ni-substitution. The layer distances of the Co-, Cu- and Zn-substituted LDHs remained equal or similar to those obtained for MgAl-LDH. The substitution of Al^{3+} by Fe^{3+} increased the $d_{(003)}$ value from 7.547 Å to 7.572 Å, as a possible result of the large difference in ionic radius of Al^{3+} (0.535 Å) and Fe^{3+} (0.645 Å).[31] The substitution of Mg^{2+} (0.72 Å) with Ni^{2+} (0.69 Å) increased the layer distance from 7.547 Å to 7.609 Å even though the Ni cation is slightly smaller than the Mg cation. It is possible that the increase in layer spacing was observed due to an increase in interlayer water. No change in layer distance was observed for Co^{2+} (0.745 Å), Zn^{2+} (0.74 Å) and Cu^{2+} (0.73 Å) substitution for Mg^{2+} (0.72 Å), which corresponds well to the fact that all four metals have a similar ionic radius. Changes in c and a parameters (where the ionic radius of the substituted metal is similar) can be ascribed to changes in interstitial water content or anion orientation/ordering. Changes in interlayer water content would be visible in the TGA curves of the sample through a peak shift in the differential curve between 150 °C and 200 °C against MgAl-LDH and will be further discussed in the TGA section.

Table 2 shows the positions of the basal planes (003), (006), (009) and (110), the corresponding d-spacing and crystal parameters as well as the estimated crystallite size (L). Table 2(b)† shows the crystal parameters for the 10% substituted LDHs and can be found in the ESI. The d-spacings were calculated using Bragg's Law. Crystal parameters c and a were calculated with $c = \frac{1}{3}(3d_{003} + 6d_{006} + 9d_{009})$ and $a = 2d_{110}$. Crystallite thicknesses (based on the (003) reflection) were estimated using the Scherrer equation $L = \frac{K\lambda}{\beta \cos\theta}$ where L is the mean size of crystalline domains parallel to the lattice plane, λ is the wavelength, K is a shape factor of 0.9 and β is the

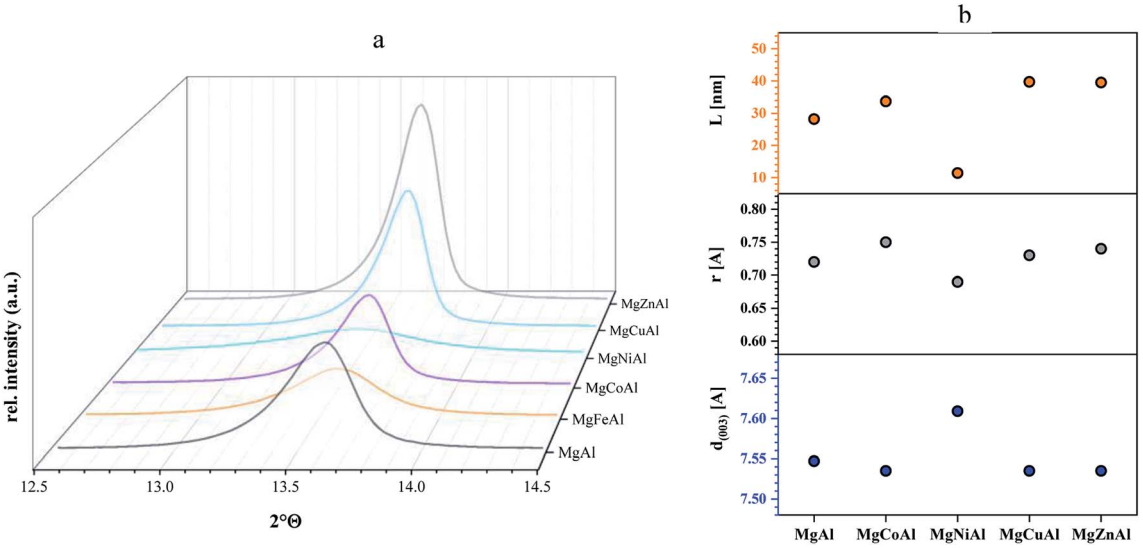

Fig. 3 (a) Detailed XRD pattern of reflex (003) for MgAl-LDH and MgMAl-LDH with M = Fe, Co, Ni, Cu, Zn (5 mol% sub.). (b) Correlation of atomic radii with d-spacing and crystallite size of MgAl-LDH substituted by 5% di-valent transition metals.

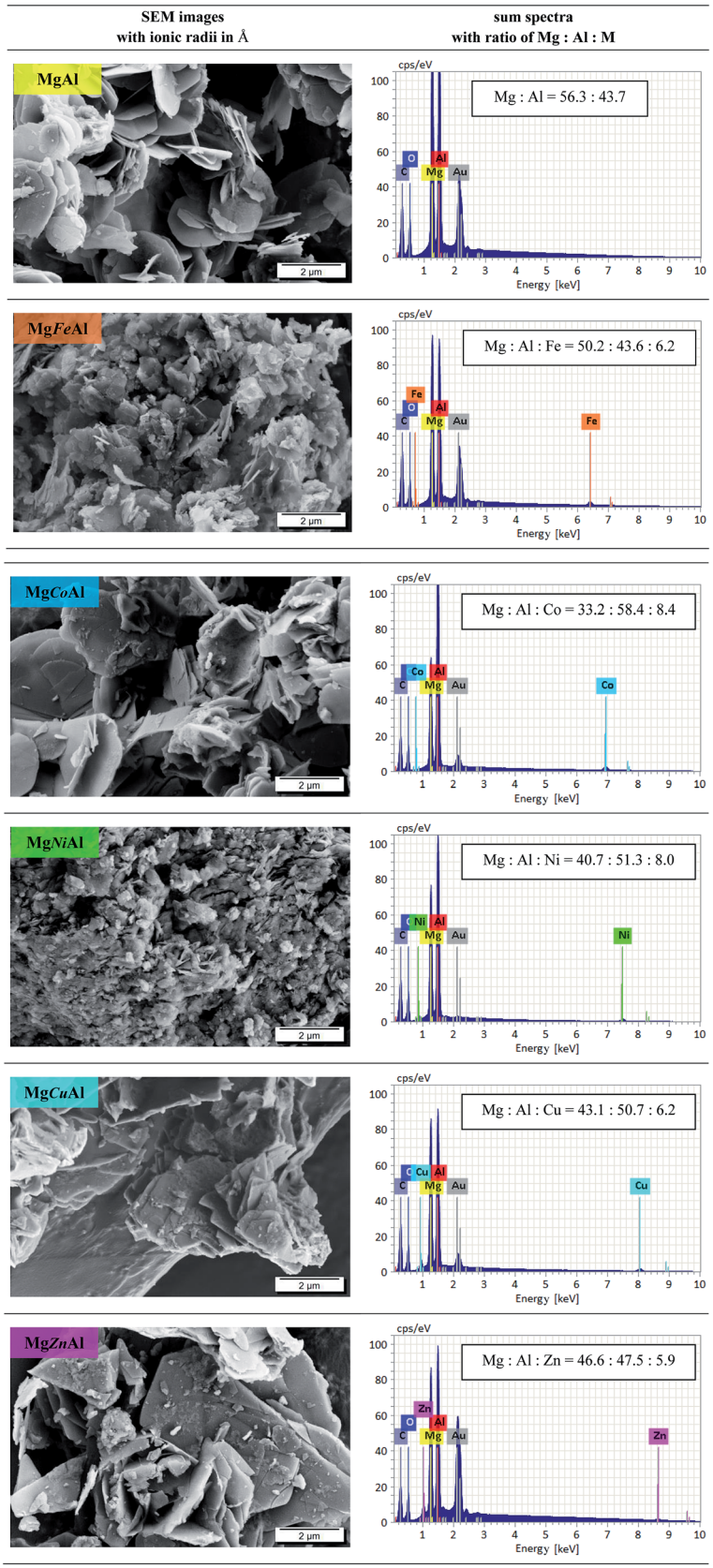

Fig. 4 SEM images of MgAl-LDH and MgMAl-LDH with M = Fe, Co, Ni, Cu, Zn (left) with the corresponding sum spectra and calculated atomic ratios of Mg : Al : M (right).

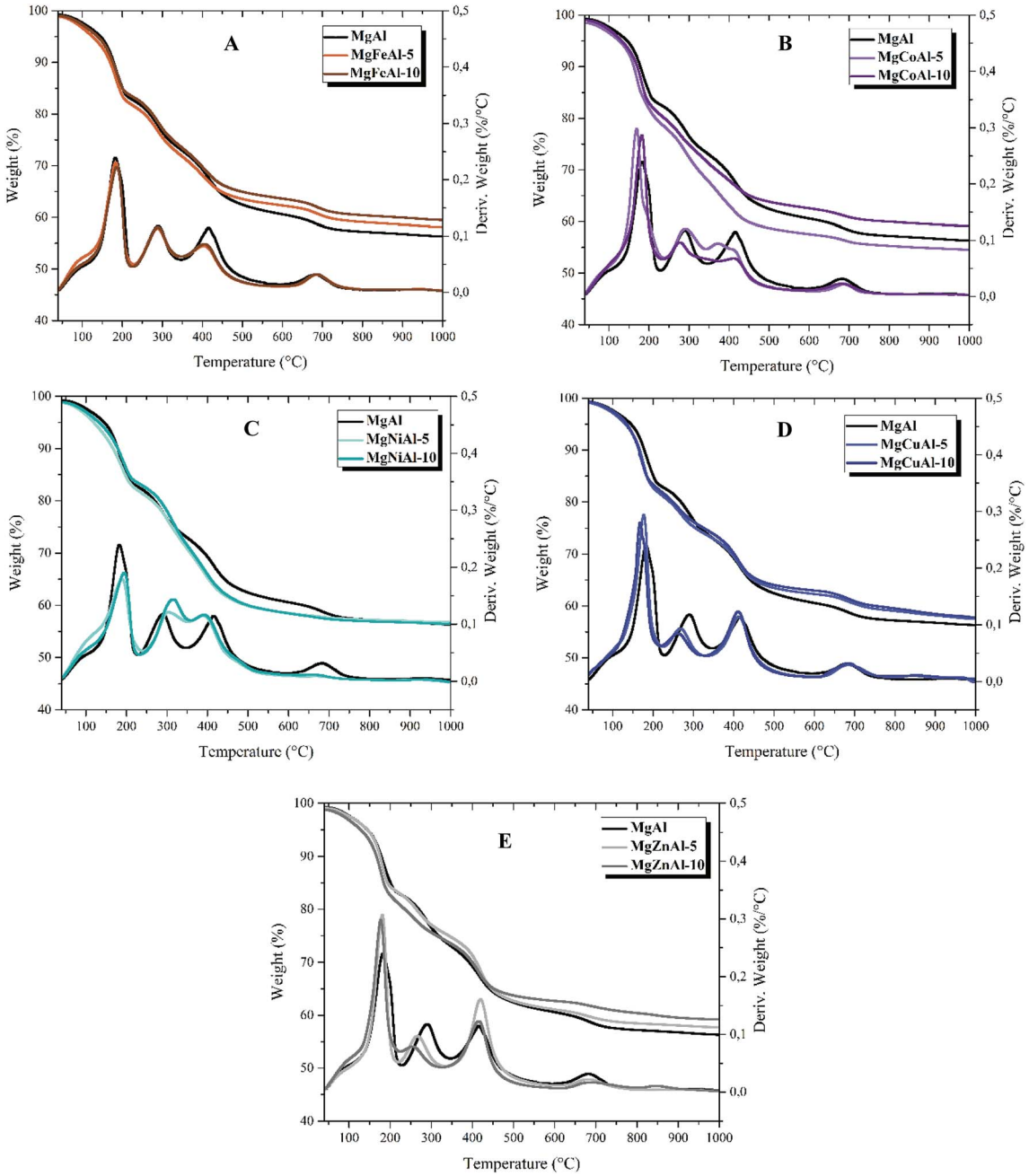

Fig. 5 TGA curves of 5% and 10% substituted tri-metal MgMAl-LDHs for the series of M = (Fe, Co, Ni, Cu, Zn), (A) MgFeAl-LDHs, (B) MgCoAl-LDHs (C), MgNiAl-LDHs, (D) MgCuAl-LDHs and (E) MgZnAl-LDHs synthesized using urea hydrolysis.

line broadening at half maximum (FWHM) of the diffraction peak. Compared to MgAl-LDH, the crystallite thickness increased for MgMAl-LDH with M = Co, Cu and Zn and decreased for MgMAl-LDH with M = Fe and Ni.

Although the crystallite thickness cannot necessarily give a direct correlation to the platelet diameter, the crystallite thicknesses show the same trend as seen for the atomic radii, whereas the calculated *d*-spacing shows the opposite trend (Fig. 3(b) for divalent transition metal substituted LDHs). It might be possible that this trend could give information regarding the number of layers of the LDH platelet with a change in transition metal – here a potential decrease in the number of layers in the order Zn > Cu > Co > Mg > Ni. It was also interesting to observe that the estimated crystallite thickness corresponded well to the observed platelet sizes in SEM. Correlations have previously been found by Galvão *et al.*[51]

Scanning electron microscopy (SEM)

Fig. 4 shows the SEM images of the synthesized MgAl- and the MgMAl-LDHs. All samples showed growth of the characteristic hexagonal platelets. The platelets were large and thin (except those obtained for Ni- and Fe-substitution) as expected for

LDHs synthesized using the urea hydrolysis method. The large dimensions of the platelets grown, stand in contrast to the small platelet size and low crystallinity of LDHs synthesized using co-precipitation. The large platelet size is a direct result of the time dependency of the hydrolysis of the urea present in the solution, which remains supersaturated to a low degree throughout precipitation.[22] The morphologies of the different transition metal substituted LDHs varied. Synthesis condition and nature of transition metal have effect on the morphology of LDHs as discussed previously. As the substitution of transition metal varied the morphology is different of MgAl LDHs.[12,26] The best defined platelet structure was obtained for plain MgAl-LDH. The platelet size decreased upon Fe- and Ni-substitution and increased upon Cu-, Co- and Zn-substitution.

Energy dispersive X-ray spectroscopy (EDX)

The EDX results (sum spectra with calculated atomic ratios of Mg : Al : M) are also shown in Fig. 4. Using EDX, SEM and XRD analysis, it could be shown that a good distribution of the transition metals in the LDHs layers could be achieved bar small amounts of residue material on the LDHs platelets. Due to the substitution of the transition metals, the ratio of Mg : Al was changed. The content of Mg decreased, whereas the amount of Al increased compared to the ratio obtained for MgAl-LDH. For the divalent transition metal substitution, the following order was found to apply for the observed Mg content: MgAl- > MgZnAl- > MgCuAl- > MgNiAl- > MgCoAl-LDH. The opposite order was observed for the Al content of the investigated sample area. The amount of the transition metal successfully incorporated into the LDH layers followed the sequence Co > Ni > Cu > Zn. Furthermore, local variations in Co distribution were observed. We believe that the decrease in Co-substitution occurred due to the formation of a layered α-$Co(OH)_2$ side-species with interstitially substituted Mg. The synthesis and application of α-$Co(OH)_2$ was studied by Rajamathi, Kamath and Seshadri (2000) and Leng *et al.*, who obtained XRD patterns very similar to those of the MgCoAl-LDH phases in this work.[52,53]

Thermogravimetric analysis (TGA)

The results of the thermal analysis obtained for the series of M = (Fe, Co, Ni, Cu, Zn) substituted tri-metal MgMAl- synthesized LDHs are shown in Fig. 5 and Table 3 (see ESI†). The series of LDHs decomposed in five stages with a total mass loss of up to 50%. The weight loss as a function of temperature is shown in Fig. 5. The obtained TGA results show a stepwise profile with five temperature regions. The first temperature region lies between 50 °C to 250 °C, the second between 250 °C and 350 °C, the third between 350 °C and 500 °C, the fourth between 500 °C to 700 °C, and the fifth between 700 °C and 1000 °C. For temperatures up to 100 °C, adsorbed water and gases are lost. The mass loss between 170 °C and 250 °C corresponds to the loss of interlayer water molecules. Between 250 °C and 500 °C the major product is CO_2 from interlayer CO_3^{2-} and water vapor formed from the dehydroxylation of OH-groups. At higher temperatures metal oxides of the LDH phase formed.[37,39,54,55] The mass loss profile and decomposition stages are summarized in Table 3.† Table 3 shows the residual weight after TGA.

The substitution of the different transition metals resulted in differences in the thermal decomposition behavior of the LDHs as can be seen in Fig. 5. Differences in thermal stability could be observed between all LDHs analyzed. It was found that the presence of different transition metals in the layers of MgAl-LDHs reduced the total weight loss. Only the 5 mol% Co-substitution increased the weight loss with respect to MgAl-LDH as can be seen in Fig. 5(B) and in Table 3.† Furthermore, it was observed that an increase in the concentration of the transition metal from 5 mol% to 10 mol% led to a decrease in total weight loss in all tested LDHs apart from MgNiAl-LDH (Fig. 5(C)). Differences in total weight loss can be explained by differences in atomic weight and concentration effects as well as changes in intermolecular forces. Finally, it could be shown that the decomposition of the LDH structure – based on the removal of interlayer carbonates (peak 2 in the DTA profile) – decreased according to MgNiAl- > MgFeAl- = MgAl- ≥ MgCoAl- > MgCuAl- > MgZnAl-LDH. An increase in transition metal content led to an increase in stability for Ni-substitution and a decrease in stability for Cu- and Zn-substitution with respect to the lower-substituted LDHs.

MgFeAl-LDH – Fig. 5(A). For Fe-substitution, the total weight loss decreased from 43.1% (MgAl-LDH) to 40.65/39.7% (MgFeAl-5/MgFeAl-10). First (up to 184/186 °C (MgFeAl-5/MgFeAl-10)), adsorbed water and gases as well as interlayer water were lost. Interlayer carbonates were decomposed up to 288/290 °C (MgFeAl-5/MgFeAl-10), and the LDH structure dehydroxylated up to 415/405 °C (MgFeAl-5/MgFeAl-10). Finally, the LDH phase was transformed to mixed oxide phases, as the hydrotalcite phase does not exist above 500 °C. Weight loss observed at higher temperatures (around 700 °C) could also have occurred as a result of the formation of Fe_2O_3.[31,37,47]

MgCoAl-LDH – Fig. 5(B). The Co-substituted LDHs provided different results to those obtained for the other LDHs. Here the weight loss of the 5 mol% substituted LDH (MgCoAl-5) was 44.0%, higher than that of MgAl-LDH with 43.1%. A decrease in total weight loss with respect to MgAl-LDH to 39.9% was observed for MgCoAl-10. Up to 169/183 °C, adsorbed water and gases as well as interlayer water was lost. Interlayer carbonates were decomposed up to 291/277 °C and the LDH structure dehydroxylated up to 372-410/410 °C. Further weight loss at higher temperatures again occurred due to the formation of

Table 3 Residual weight after TGA for different MgMAl LDHs with M = (Fe, Co, Ni, Cu, Zn) (5 mol% and 10 mol% subs.)

	Residual weight left (%)	
LDHs	5 mol%	10 mol%
MgAl	55.2 ± 2.93	55.2 ± 2.93
MgFeAl	58.6 ± 0.43	59.9 ± 0.46
MgCoAl	55.0 ± 0.26	59.2 ± 0.69
MgNiAl	56.6 ± 0.49	57.1 ± 0.15
MgCuAl	58.4 ± 0.60	58.8 ± 0.63
MgZnAl	57.9 ± 0.55	59.5 ± 0.78

Table 4 Thermogravimetric analysis data of MgMAl LDHs with M = (Fe, Co, Ni, Cu, Zn) synthesized using urea hydrolysis showing measured residue value and theoretically calculated reside value

LDHs	Theoretical residue structure (mix oxides)	Theoretical residue (%)	Measured residue (%)	Variance from theoretical residue (%)
MgAl	$4MgO \cdot Al_2O_3$	57.1	56.9	0.2
MgFeAl-5	$4MgO \cdot (Al_{0.95}Fe_{0.05})_2O_3$	57.6	59.3	−1.7
MgFeAl-10	$4MgO \cdot (Al_{0.9}Fe_{0.1})_2O_3$	58.1	60.3	−2.2
MgCoAl-5	$4(Mg_{0.95}Co_{0.05})O \cdot Al_2O_3$	60.7	56.0	4.7
MgCoAl-10	$4(Mg_{0.9}Co_{0.1})O \cdot Al_2O_3$	61.3	61.1	0.2
MgNiAl-5	$4(Mg_{0.95}Ni_{0.05})O \cdot Al_2O_3$	60.7	58.1	2.6
MgNiAl-10	$4(Mg_{0.9}Ni_{0.1})O \cdot Al_2O_3$	61.3	57.6	3.7
MgCuAl-5	$4(Mg_{0.95}Cu_{0.05})O \cdot Al_2O_3$	60.8	58.3	2.5
MgCuAl-10	$4(Mg_{0.9}Cu_{0.1})O \cdot Al_2O_3$	61.5	58.3	3.5
MgZnAl-5	$4(Mg_{0.95}Zn_{0.05})O \cdot Al_2O_3$	60.8	58.5	2.3
MgZnAl-10	$4(Mg_{0.9}Zn_{0.1})O \cdot Al_2O_3$	61.5	60.5	1.0

mixed metal oxides from the LDH phase.[39] Similar results were obtained in the study of the influence of Co-substitution in MgAl-LDHs.[39,43,47]

MgNiAl-LDH – Fig. 5(C). For Ni-substitution, the total weight loss decreased to 41.9/42.4% from 43.1%. MgNiAl-LDH showed a sharp increase in weight loss between 200 °C and 400 °C. Interlayer water and adsorbed gases were lost until 190/195 °C. Interlayer carbonates were decomposed up to 304/315 °C and the LDH structure dehydroxylated up to 390/392 °C. Decomposition of hydroxyl groups and carbonate anions occurred until 668/658 °C. Further weight loss at higher temperatures around 700 °C in Fig. 5(C) occurred due to the formation of transition metal oxides. Similar thermal decomposition behavior was observed by Chmielarz *et al.* and Curtius *et al.*[39,47]

MgCuAl-LDH – Fig. 5(D). The total weight loss for the Cu-substituted LDHs was the same for both substitution percentages (41.7%) and less than that of MgAl-LDH (43.1%). In Fig. 5(D), it can be seen that the interlayer water was lost at lower temperatures compared to MgAl-LDH. Adsorbed water and gases as well as interlayer water were lost until 177/168 °C. Interlayer carbonates were decomposed up to 262/268 °C and the LDH structure dehydroxylated up to 413/410 °C. The peak at 849 °C in the case of 5 mol% Cu-substituted and 858 °C in the case of the 10 mol% Cu-substituted LDHs could have occurred due to the thermal reduction of Cu. Similar behavior was observed at 860 °C in a previous study by Chmielarz *et al.*, who synthesized CuMgAl-LDH using co-precipitation.[39] It seems that Cu is responsible for stabilization of MgAl-LDHs.

MgZnAl-LDH – Fig. 5(E). The total weight loss for the Zn-substituted LDHs decreased to 41.5/39.5% from 43.1% for MgAl-LDH. The substituted LDHs decomposed at lower temperatures than MgAl-LDH. Adsorbed water and gases as well as interlayer water were lost up to 181/178 °C. Interlayer carbonates were decomposed up to 267/254 °C and the LDH structure dehydroxylated up to 420/415 °C. Further weight loss at higher temperatures around 700 °C occurred due to the formation of a mixed oxide phase. Wang *et al.* and Sakr *et al.* studied the synthesis of ZnMgAl-LDHs but did not discuss the effect of the substitution on their thermal decomposition.[36,44]

As a comparison it can be seen that substitution of different transition metals in MgAl-LDHs have effect on thermal stability of MgAl LDHs. Different morphology and structure can also be observed from the XRD and SEM analysis for different substitution of transition metal in MgAl LDHs.

Comparison of theoretical residual weight and measured residual weight of different LDHs

The residual weight after complete calcination of LDHs (into a mixed oxide) can be calculated from eqn (2) as previously given by Forano *et al.*[56] The decomposition follows approximately through this equation, although other decomposition phases are possible dependent on the composition of LDHs. For the carbonate intercalated LDHs investigated in this article the anion decomposition product is expected to be CO_2.

$$\left[M_{(1-x)}{}^{2+}M_x{}^{3+}(OH)_2\right]^{x+} \cdot \left[A_{x/q}{}^{q-}nH_2O\right]^{x-} \xrightarrow{\Delta} (1-x)$$

$$M^{2+}O \cdot xM_2{}^{3+}O_3 + yH_2O + \text{interlayer decomposition product} \quad (2)$$

It is assumed that eqn (2) can also be used when calculating the residual weights of the synthesized tri-metal LDHs – if similar decomposition products are formed. A comparison between theoretical residual weights calculated under this assumption and the measured residual weights obtained through TGA is presented in Table 4. No large deviations in residual weight from the theoretical values were observed in any of the samples.

No clear correlation between the residual weights and other analyses results were observed. However, there appears to be a correlation between the variance of the theoretical residual weight and measured residual weight (indicated as percentage variance from theoretical residue in Table 4) when compared to the incomplete substitution as observed through EDX analysis. From the results it appears that the lower the variance from the theoretical residual weight, the higher the substitution efficiency. If the atomic substitution did not occur as expected, it is likely that some of the expected LDH phase would not have formed (in favor of other metal complexes), thus leading to a decrease in the measured residual weight. In the case of trivalent metal substitution (partially replacing the Al with Fe),

the measured residue was more than the postulated theoretical value. This may be attributed to the higher Mg content of the LDH phase or an increase in interstitial water content.

Conclusion

A comprehensive understanding of LDHs is important for their future applications as catalyst and flame retardants. Co-precipitation, hydrothermal and modified urea hydrolysis methods as well as a variety of metal combinations have been studied previously. In this study, the urea hydrolysis method was (for the first time comprehensively) used for the preparation of Fe-, Co-, Ni-, Cu- and Zn-substituted MgAl-LDH at the same synthesis conditions, allowing true comparison between the LDH properties with respect to morphology and changes in thermal decomposition behavior. The LDHs were studied using XRD, SEM, SEM-EDX and TGA.

Well defined crystals with hexagonal platelet structure and large platelet size were obtained. Good distribution of the transition metal in the MgAl-LDH layers could be achieved at 5 mol% substitution. The different substituted transition metals had a notable effect on the morphology and platelet size. The substitution percentage had a notable effect on thermal behavior. It might be valuable to further investigate the effect of an increasing substitution percentage in future. In conclusion, the urea hydrolysis method provides a simple one pot synthesis method for tri-metal LDHs that could find applications in different research areas. It is envisaged that other tri-metal combinations of LDHs could be synthesized using this method and their properties further investigated.

Conflicts of interest

There are no conflicts to declare.

Acknowledgements

We acknowledge the Leibniz Institut für Polymerforschung Dresden e. V., Germany for providing the facilities to do this research. Sajid Naseem is also thankful to the Higher Education Commission (HEC), Pakistan and German Academic Exchange Service (DAAD) for providing his scholarship. The authors would also like to thank Techsparks (Pty) Ltd and the Technology and Human Resources for Industry Programme (THRIP) administered by the Department of Trade and Industry, South Africa, (grant number THRIP/133/31/03/2016) for their contribution in terms of funding for powder X-ray diffraction analysis performed at the University of Pretoria, South Africa and a travel allowance for Bianca Gevers to visit the Institut für Polymerforschung Dresden e. V to work on this project. Bianca Gevers is also thankful to the Institut für Polymerforschung Dresden e. V. for providing her guest student stipend for the duration of her stay.

References

1 Y. Kuang, L. Zhao, S. Zhang, F. Zhang, M. Dong and S. Xu, *Materials*, 2010, **3**, 5220–5235.
2 In *Modern Inorganic Synthetic Chemistry*, ed. R. Xu and Y. Xu, Elsevier, Amsterdam, 2nd edn, 2017, pp. 493–543, DOI: 10.1016/B978-0-444-63591-4.00018-5.
3 J. Yu, Q. Wang, D. O'Hare and L. Sun, *Chem. Soc. Rev.*, 2017, **46**, 5950–5974.
4 S. P. Lonkar, A. Leuteritz and G. Heinrich, *RSC Adv.*, 2013, **3**, 1495–1501.
5 B. Kutlu, A. Leuteritz, L. Häußler, U. Oertel and G. Heinrich, *Polym. Degrad. Stab.*, 2014, **102**, 9–14.
6 S. Naseem, S. P. Lonkar, A. Leuteritz and F. J. W. J. Labuschagné, *RSC Adv.*, 2018, **8**, 29789–29796.
7 Y. Gao, J. Wu, Q. Wang, C. A. Wilkie and D. O'Hare, *J. Mater. Chem. A*, 2014, **2**, 10996–11016.
8 S.-J. Xia, F.-X. Liu, Z.-M. Ni, W. Shi, J.-L. Xue and P.-P. Qian, *Appl. Catal., B*, 2014, **144**, 570–579.
9 J. J. Reinosa, P. Leret, C. M. Álvarez-Docio, A. del Campo and J. F. Fernández, *Bol. Soc. Esp. Ceram. Vidrio*, 2016, **55**, 55–62.
10 F. L. Theiss, G. A. Ayoko and R. L. Frost, *Appl. Surf. Sci.*, 2016, **383**, 200–213.
11 R. Quispe-Dominguez, S. Naseem, A. Leuteritz and I. Kuehnert, *RSC Adv.*, 2019, **9**, 658–667.
12 U. Costantino, F. Marmottini, M. Nocchetti and R. Vivani, *Eur. J. Inorg. Chem.*, 1998, **1998**, 1439–1446.
13 E. N. Kalali, X. Wang and D.-Y. Wang, *J. Mater. Chem. A*, 2016, **4**, 2147–2157.
14 D. Basu, A. Das, D.-Y. Wang, J. J. George, K. W. Stockelhuber, R. Boldt, A. Leuteritz and G. Heinrich, *RSC Adv.*, 2016, **6**, 26425–26436.
15 Y. Peng, W. Wang, J. Cao and Y. Huang, *J. Appl. Polym. Sci.*, 2017, **134**, 44597.
16 B. Nagendra, C. V. S. Rosely, A. Leuteritz, U. Reuter and E. B. Gowd, *ACS Omega*, 2017, **2**, 20–31.
17 Y. Zhu, R. Zhu, G. Zhu, M. Wang, Y. Chen, J. Zhu, Y. Xi and H. He, *Appl. Surf. Sci.*, 2018, **433**, 458–467.
18 Y. Cao, P. Maitarad, M. Gao, T. Taketsugu, H. Li, T. Yan, L. Shi and D. Zhang, *Appl. Catal., B*, 2018, **238**, 51–60.
19 J. An, L. Shi, G. Chen, M. Li, H. Liu, S. Yuan, S. Chen and D. Zhang, *J. Mater. Chem. A*, 2017, **5**, 19738–19744.
20 Z. Chen, Z. Tao, S. Cong, J. Hou, D. Zhang, F. Geng and Z. Zhao, *Chem. Commun.*, 2016, **52**, 11442–11445.
21 G. Chen, J. An, Y. Meng, C. Yuan, B. Matthews, F. Dou, L. Shi, Y. Zhou, P. Song, G. Wu and D. Zhang, *Nano Energy*, 2019, **57**, 157–165.
22 J. He, M. Wei, B. Li, Y. Kang, D. G. Evans and X. Duan, in *Layered Double Hydroxides*, ed. X. Duan and D. G. Evans, Springer Berlin Heidelberg, Berlin, Heidelberg, 2006, pp. 89–119, DOI: 10.1007/430_006.
23 J. S. Valente, M. S. Cantu and F. Figueras, *Chem. Mater.*, 2008, **20**, 1230–1232.
24 J. S. Valente, M. Sánchez-Cantú, E. Lima and F. Figueras, *Chem. Mater.*, 2009, **21**, 5809–5818.

25 D.-K. Cho, C.-W. Jeon and I.-K. Park, *J. Alloys Compd.*, 2018, **737**, 725–730.
26 J. J. Bravo-Suárez, E. A. Páez-Mozo and S. T. Oyama, *Quim. Nova*, 2004, **27**, 601–614.
27 C. Forano, U. Costantino, V. Prévot and C. T. Gueho, in *Developments in Clay Science*, ed. F. Bergaya and G. Lagaly, Elsevier, 2013, vol. 5, pp. 745–782.
28 F. Cavani, F. Trifirò and A. Vaccari, *Catal. Today*, 1991, **11**, 173–301.
29 S. MIYATA, *Clays Clay Miner.*, 1980, **28**, 50–56.
30 M. Pavlovic, P. Rouster, T. Oncsik and I. Szilagyi, *ChemPlusChem*, 2017, **82**, 121–131.
31 K. Parida, M. Satpathy and L. Mohapatra, *J. Mater. Chem.*, 2012, **22**, 7350–7357.
32 H. T. Kang, K. Lv and S. L. Yuan, *Appl. Clay Sci.*, 2013, **72**, 184–190.
33 J. Wang, T. Zhang, M. Li, Y. Yang, P. Lu, P. Ning and Q. Wang, *RSC Adv.*, 2018, **8**, 22694–22709.
34 M. Jabłońska, L. Chmielarz, A. Węgrzyn and S. WITKOWSKI, *Chemik*, 2012, **66**, 750–757.
35 S. Basąg, Z. Piwowarska, A. Kowalczyk, A. Węgrzyn, R. Baran, B. Gil, M. Michalik and L. Chmielarz, *Appl. Clay Sci.*, 2016, **129**, 122–130.
36 G. Wang, M. Yang, Z. Li, K. Lin, Q. Jin, C. Xing, Z. Hu and D. Wang, *J. Nanopart. Res.*, 2013, **15**, 1882.
37 L. Chmielarz, M. Jabłońska, A. Strumiński, Z. Piwowarska, A. Węgrzyn, S. Witkowski and M. Michalik, *Appl. Catal., B*, 2013, **130–131**, 152–162.
38 F. Kovanda, K. Jirátová, J. Rymeš and D. Koloušek, *Appl. Clay Sci.*, 2001, **18**, 71–80.
39 L. Chmielarz, P. Kuśtrowski, A. Rafalska-Łasocha and R. Dziembaj, *Thermochim. Acta*, 2002, **395**, 225–236.
40 S. Kim, J. Fahel, P. Durand, E. André and C. Carteret, *Eur. J. Inorg. Chem.*, 2017, **2017**, 669–678.
41 Z. Liu, R. Ma, Y. Ebina, N. Iyi, K. Takada and T. Sasaki, *Langmuir*, 2007, **23**, 861–867.
42 Y.-M. Zheng, N. Li and W.-D. Zhang, *Colloids Surf., A*, 2012, **415**, 195–201.
43 L. H. Chagas, G. S. G. De Carvalho, W. R. Do Carmo, R. A. S. San Gil, S. S. X. Chiaro, A. A. Leitão, R. Diniz, L. A. De Sena and C. A. Achete, *Mater. Res. Bull.*, 2015, **64**, 207–215.
44 A. A. E. Sakr, T. Zaki, O. Elgabry, M. A. Ebiad, S. M. El-Sabagh and M. M. Emara, *Appl. Clay Sci.*, 2018, **160**, 263–269.
45 F. J. W. J. Labuschagne, D. M. Molefe, W. W. Focke, I. van der Westhuizen, H. C. Wright and M. D. Royeppen, *Polym. Degrad. Stab.*, 2015, **113**, 46–54.
46 A. Tsyganok and A. Sayari, *J. Solid State Chem.*, 2006, **179**, 1830–1841.
47 H. Curtius, G. Kaiser, K. Rozov, A. Neumann and D. Kathy Dardenne, *Clays Clay Miner.*, 2013, **61**, 424–439.
48 N. Iyi and T. Sasaki, *J. Colloid Interface Sci.*, 2008, **322**, 237–245.
49 R. Dohrmann, K. B. Rüping, M. Kleber, K. Ufer and R. Jahn, *Clays Clay Miner.*, 2009, **57**, 686–694.
50 Database of Ionic Radii, http://abulafia.mt.ic.ac.uk/shannon/radius.php, accessed 23/07/2018.
51 T. L. P. Galvão, C. S. Neves, A. P. F. Caetano, F. Maia, D. Mata, E. Malheiro, M. J. Ferreira, A. C. Bastos, A. N. Salak, J. R. B. Gomes, J. Tedim and M. G. S. Ferreira, *J. Colloid Interface Sci.*, 2016, **468**, 86–94.
52 M. Rajamathi, P. V. Kamath and R. Seshadri, *Mater. Res. Bull.*, 2000, **35**, 271–278.
53 X. Leng, K.-H. Wu, Q. Zeng, I. R. Gentle and D.-W. Wang, *Asia-Pac. J. Chem. Eng.*, 2016, **11**, 415–423.
54 R. Chitrakar, S. Tezuka, A. Sonoda, K. Sakane and T. Hirotsu, *Ind. Eng. Chem. Res.*, 2008, **47**, 4905–4908.
55 V. R. Choudhary, R. Jha and P. A. Choudhari, *J. Chem. Sci.*, 2005, **117**, 635–639.
56 C. Forano, T. Hibino, F. Leroux and C. Taviot-Guého, in *Developments in Clay Science*, ed. F. Bergaya, B. K. G. Theng and G. Lagaly, Elsevier, 2006, vol. 1, pp. 1021–1095.